Final Report for SCEC project, "Towards Forecasting Directivity on Southern California Faults: Testing Model Seismicity and Directivity Correlations with Southern California Data" 2006, $33,000, PI: B.E. Shaw

The main thrust of this work is to seek a deeper understanding of the dynamics of earthquakes on fault systems and its relationship to seismic hazard. A key question is how much of the directivity and extent of dynamic ruptures can be anticipated, in particular from seismicity and fault geometry. Results from support of this grant are still being developed. In the last year, four papers have been published. Below, some results of the papers most directly relevant to this project are briefly mentioned.

"Initiation propagation and termination of elastodynamic ruptures associated with segmentation of faults and shaking hazard", [Shaw, 2006], *Journal of Geophysical Research , 111*, **B07304, doi:10.1029/2005JB0040077** . Using a model of a complex fault system, we examine the initiation, propagation, and termination of ruptures, and their relationship to fault geometry and shaking hazard. We find concentrations of epicenters near fault stepovers and ends; concentrations of terminations near fault ends; and persistent propagation directivity effects. Taking advantage of long sequences of dynamic events, we directly measure shaking hazards, such as peak ground acceleration exceedance probabilities, without need for additional assumptions. This provides a new tool for exploring shaking hazard from a physics-based perspective, its dependence on various physical parameters, and its correlation with other geological and seismological observables. Using this capability, we find some significant aspects of the shaking hazard can be anticipated by measures of the epicenters. In particular, asymmetries in the relative peak ground motion hazard along the faults appear well correlated with asymmetries in epicentral locations.

Figure 1 shows three different views of the complex sequences which develop, and the long catalogue of dynamic ruptures which occur on it. Figure 1a shows the slip rate on each of the faults, greyscaled proportional to slip rate. We see very interesting patterns of linked segments, and smaller faults associated with large segment stepovers and ends. These smaller faults help accommodate deformation, keeping stresses finite with accumulating strain. The dynamic ruptures which occur on these complex fault systems have interesting relationships with the fault geometry. Figure 1b shows the density of epicenters for a long sequence of dynamic events on this fault system. Interestingly, the epicenters occur both along the main faults, where slip has been concentrated, and along the minor linking faults off of the main faults where little slip has occurred. Ruptures initiating on these minor faults can sometimes jump onto larger adjacent segments and grow into large ruptures, so they play a non-negligible role in the hazard. Figure 1c shows the density of rupture terminations, where the two terminations of each rupture are defined as the farthest points ruptured on either side of the epicenters. They are strongly associated with segment ends, and are even more concentrated than the epicenters.

In addition to the initiation and termination, the propagation of ruptures is also strongly influenced by the fault geometry. We see persistent directivity effects on most of the fault system. Figure 1d shows the fraction of ruptures propagating in either direction, colorscaled with blue for up and red for down, with the fraction defined by $f = (N_{up} - N_{down})/(N_{up} + N_{down})$ so $-1 \leq f \leq 1$. Here N_{up} is the number of times a point breaks during a rupture event with the rupture locally propagating upwards, while N_{down} is similarly when it is locally propagating downwards. Note the dearth of neutral green colors in the figure where the propagation fraction is near zero, meaning only rarely do locations not have a preferred propagation direction.

In addition to giving us insight into rupture dynamics processes, directivity plays an important role in hazard. Rupture directivity makes a big difference in ground motions, amplifying or decreasing motions by severalfold, depending on whether the rupture is propagating towards or away from a location. Indeed, we can look directly at some hazard measures of shaking in the model, and see these effects. Taking advantage of the fully dynamic nature of the simulation, we measure directly for each event various shaking measures. Utilizing a long catalogue of dynamic events, we can make a hazard map for the fault system, combining thousands of dy-

namic ruptures measured individually. Figure 2a plots a standard measure of hazard, the peak acceleration for a given probability of occurrence. We measure this in the model by keeping track of peak acceleration at every point in space from each event, combining all the events to make at every point a histogram of these values. Then, choosing a probability value, we plot the acceleration level at which that probability value is exceeded over the long catalogue.

Figure 2b shows the peak velocity for the same probability of occurrence as in Figure 2a (the analogue of the 2% probability of exceedance in 50 year national hazard maps [see also http://eqhazmaps.usgs.gov]). Note the strong similarity with Figure 2a, albeit slightly less concentrated near the faults.

The last measure of shaking we show in Figure 2c is the average of kinetic energy. Note, in contrast with the peak motion curves in Figures 2a and 2b, the kinetic energy is much more symmetric along the fault, and much more concentrated along the largest faults. Thus Figure 2c is best anticipated by Figure 1a, the total slip rate on faults. The shaking maps, on the other hand, reflect rupture initiation, propagation, and termination effects in Figures 1b, 1c, and Figure 1d .

Being able to directly measure the hazard, as opposed to constructing it from parameterizations, we wan look for correlations which are not built in. One virtue of having these long synthetic catalogues, on which we can examine details of dynamic ruptures, is we can examine relationships between quantities which may be less easily obtained with observations. Indeed, some significant aspects of the shaking hazard can be anticipated from aspects of the model which have observable geological and seismological analogues. Figure 3 suggests that the asymmetry in the shaking along a fault may be one such measure.

In Figure 3a, we consider a geological observable, the distance weighted asymmetry in the slip on the two halves of a fault segment. We plot for each segment the slip asymmetry on the horizontal axis and the peak acceleration average asymmetry on the vertical axis (peak acceleration is averaged on both adjacent sides of the fault, since, as the dark lines in Figure 2a located where the main faults are indicate, the symmetry at the fault leaves the shaking right on the fault quite small). We find a significant correlation, with $R^2 = .45$, so that nearly half of the variance of this shaking hazard asymmetry is accounted for by a geological measure.

We can do even better with a seismological observable, the asymmetry in the position of epicenters. In Figure 3b we plot on the horizontal axis the average position of the epicenters relative to the center of the segment, and on the vertical axis the same acceleration asymmetry as before Again we see a strong correlation, this time with an even higher $R^2 = .79$. This correlation occurs because of directivity effects: the highest accelerations occur as a large rupture is moving towards you, and since ruptures propagate away from their epicenters, the shaking near the epicenters is lower than the shaking farther down the fault. Measurements from the dense array of recordings from the recent 2004 Parkfield M6.0 earthquake illustrate this well [http://www.quake.ca.gov/cisn-edc/IQR/Parkfield_28Sep2004/parkfield_shaking.pdf]. We have checked this correlation with a range of lower magnitude cutoff values for the seismicity, shown with different symbols in Figure 3b, and found similar results independent of the magnitude cutoff. This is good news, suggesting we may be able to use the spatial distribution of the numerous small earthquakes, together with mapped fault geometries, to anticipate aspects of rupture directivity and shaking hazard, which is dominated by the rare larger earthquakes.

" Relation between stress heterogeneity and aftershock rate in the rate-and-state model", [Helmstetter and Shaw, 2006], *Journal of Geophysical Research , 111*, **B07304, doi:10.1029/ 2005JB0040077.** We estimate the rate of aftershocks triggered by a heterogeneous stress change, using the rate-and-state model of *Dieterich* [1994]. We show than an exponential stress distribution $P(\tau) \sim \exp(-\tau/\tau_0)$ gives an Omori law decay of aftershocks with time $\sim 1/t^p$, with an exponent $p = 1 - A\sigma_n/\tau_0$, where A is a parameter of the rate-and-state friction law, and σ_n the normal stress. Omori exponent p thus decreases if the stress "heterogeneity" τ_0 decreases. We also invert the stress distribution $P(\tau)$ from the seismicity rate $R(t)$, assuming that the stress does not change with time. We apply this method to a synthetic stress map, using the (modified) scale invariant "k^2" slip model [Herrero and Bernard, 1994]. We generate synthetic aftershock catalogs from this stress change. The seismicity rate on the rupture area shows a

huge increase at short times, even if the stress decreases on average. Aftershocks are clustered in the regions of low slip, but the spatial distribution is more diffuse than for a simple slip dislocation. Because the stress field is very heterogeneous, there are many patches of positive stress changes everywhere on the fault. This stochastic slip model gives a Gaussian stress distribution, but nevertheless produces an aftershock rate which is very close to Omori's law, with an effective $p \leq 1$, which increases slowly with time. The inversion of the full stress distribution $P(\tau)$ is badly constrained for negative stress values, and for very large positive values, if the time interval of the catalog is limited. However, constraining $P(\tau)$ to be a Gaussian distribution allows a good estimation of $P(\tau)$ for a limited number of events and catalog duration. We show that stress shadows are very difficult to observe in a heterogeneous stress context.

"Impact of Friction and Scale-Dependent Initial Stress on Radiated Energy-Moment Scaling", [Shaw, 2006b], in Abercrombie et al, eds, 'Earthquakes: Radiated Energy and the Physics of Faulting', *AGU Geophysical Monograph Series, Volume 170* . The radiated energy coming from an event depends on a number of factors, including the friction and, crucially, the initial stress. Thus we cannot deduce any scaling laws without considering initial stress. However, by simulating long sequences of events, where the system evolves to a statistically steady-state, we can obtain the appropriate distribution of initial stresses consistent with the dynamics and a given friction. We examine a variety of frictions, including power-law slip dependence, and explore a variety of scaling relations, with the aim of elucidating their radiated energy-moment scaling. We find, contrary to expectations, that apparent stress is not seen to increase with earthquake size for power-law weakening. For small and for large events, little change in apparent stress is seen with increasing rupture size, while intermediate sized events interpolate in between. We find the origin of this unexpected lack of size dependence in systematic changes of initial stress, with bigger events tending to sample regions of lower initial stress. To understand radiated energy-moment scaling, scale-dependent initial stress needs to be considered.

"Probabilities for jumping fault segment stepovers", [Shaw, B.E. and J.H. Dieterich, 2007], *Geophysical Research Letters, 34* **L01307, doi:10.1029/2006GL027980** . Seismic hazard analysis relies heavily on the segmentation of faults. The ability of ruptures to break multiple segments has a big impact on estimated hazard. Current practice for estimating multiple segment breakage relies on panels of experts voting on their opinions for each case. Here, we explore the probability of elastodynamic ruptures jumping segment stepovers in numerical simulations of segmented fault systems. We find a simple functional form for the probability of jumping a segment stepover as a function of stepover distance: an exponential falloff with distance. We suggest this simple parameterization of jumping probabilities, combined with sparse observational data to fix the lengthscale parameter, as a new approach to estimating multisegment earthquake hazard.

Figure 4a shows the probability of jumping a segments stepover for all the pairs of segments as a function of stepover separation distance. It shows as well a mean fit to the probability.

Plotting the log of the jump probability versus the linear distance of separation, Figure 4b shows a key result: the jump probability is seen to fall off exponentially at short distances, followed by a slower exponential falloff at larger distances. Specifically, we find

$$p(r) = e^{-r/r_0} + \epsilon(e^{-r/r_1} - e^{-r/r_0}) \tag{1}$$

is a good fit to the probability p distribution dependence on distance r, with $\epsilon \ll 1$ and $r_0 < r_1$. This provides a one parameter fit r_0 at short distances, a fitting which is likely to be sufficient for hazard purposes. A further fit of a constant level ϵ at intermediate distances $r_0 < r < r_1$, and r_1 at large distances $r_1 < r$ can be made as well. Note that the probability distribution has the important continuity property tha t at zero distance the jump probability is unity.

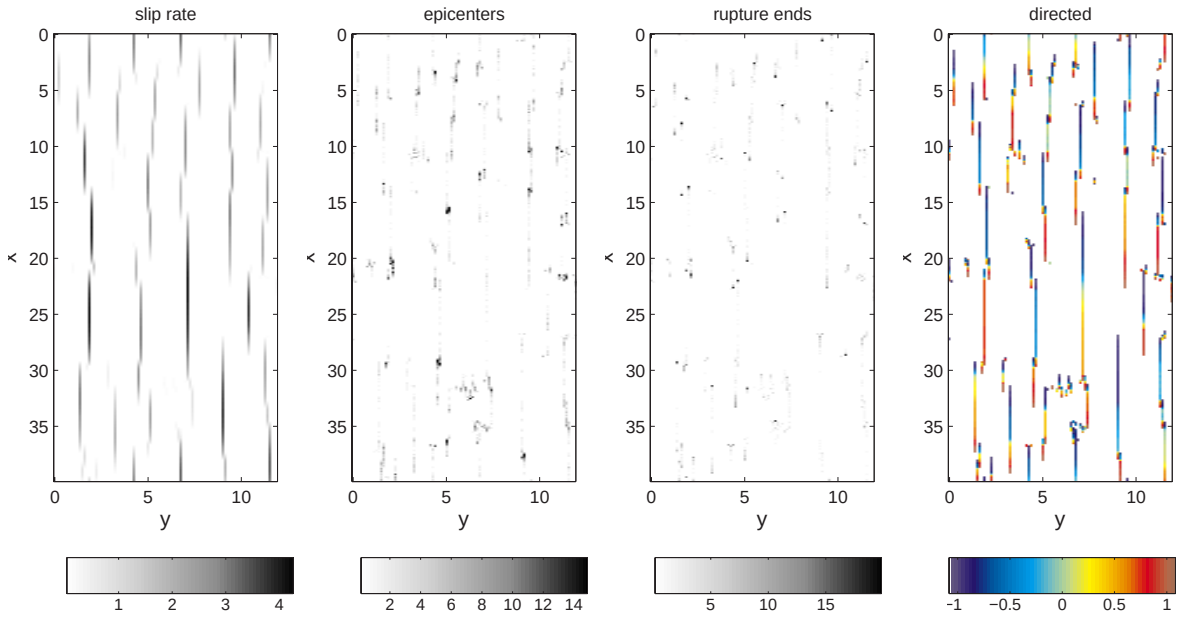

Figure 1: Three views of a long catalogue of events. (a) Slip rate per unit strain. (b) Epicentral density. (c) Rupture termination density. (d) Directivity of ruptures; fraction of events propagating up (blue colors) versus down (red colors). Note the association of epicenters with segment stepovers and ends, and the association of rupture terminations with segment ends. Note, in (d), high amplitudes– persistent directivity– is the typical, rather than exceptional case. Numbers on the horizontal and vertical axes are distances in units of the brittle crust depth, corresponding to unscaled lengths of order a few hundred km across by a thousand km long. Scale bars below the figures indicate greyscale levels.

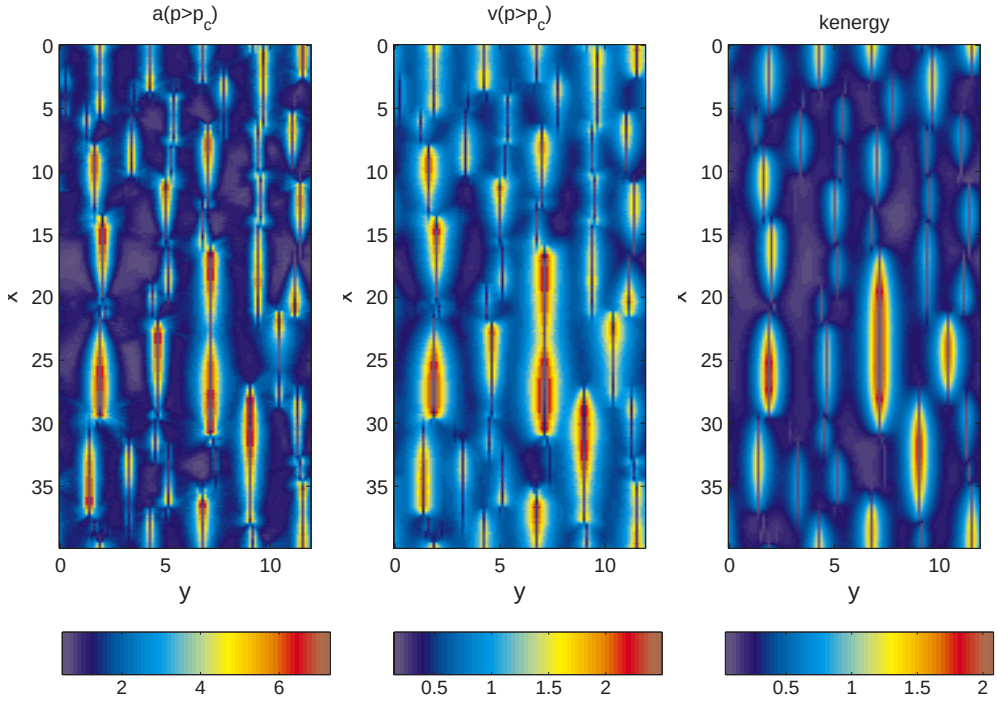

Figure 2: Shaking measures measured directly from long sequence of dynamic events. (a) Peak acceleration for $p > p_c$, with $p_c = .2$. (b) Peak velocity for $p > p_c$, with $p_c = .2$. (c) Kinetic energy. Note similar maps of peak accelerations and peak velocity, showing significant directivity effects, as contrasted with the more symmetric kinetic energy map.

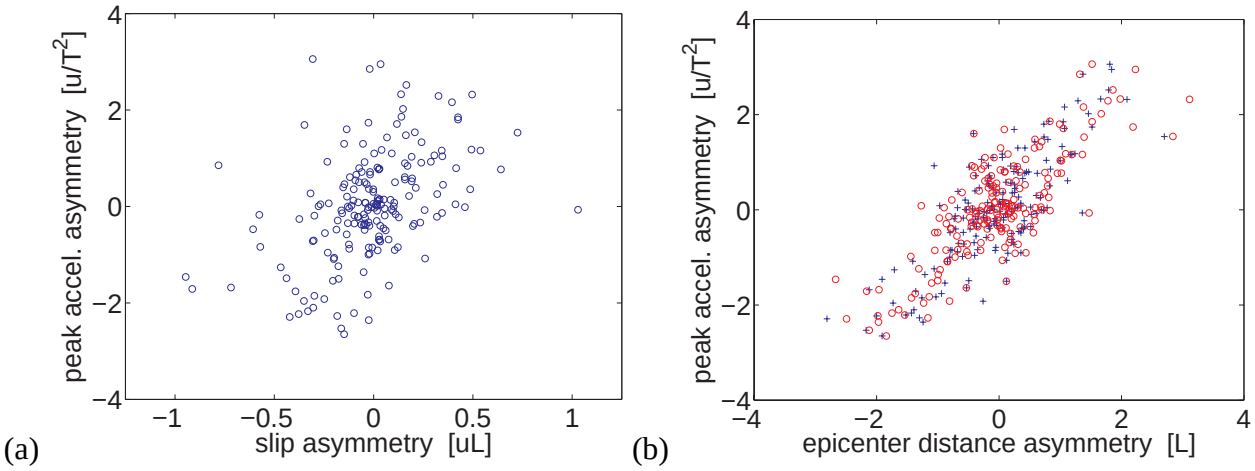

Figure 3: Correlation of asymmetry in peak acceleration on a segment with geological and seismological measures on a segment. (a) Peak acceleration asymmetry versus slip asymmetry. (b) Peak acceleration asymmetry versus epicenter location asymmetry. Blue crosses are using epicenters of small magnitude and larger events, red circles are using epicenters of large events only; both do well at explaining the trend.

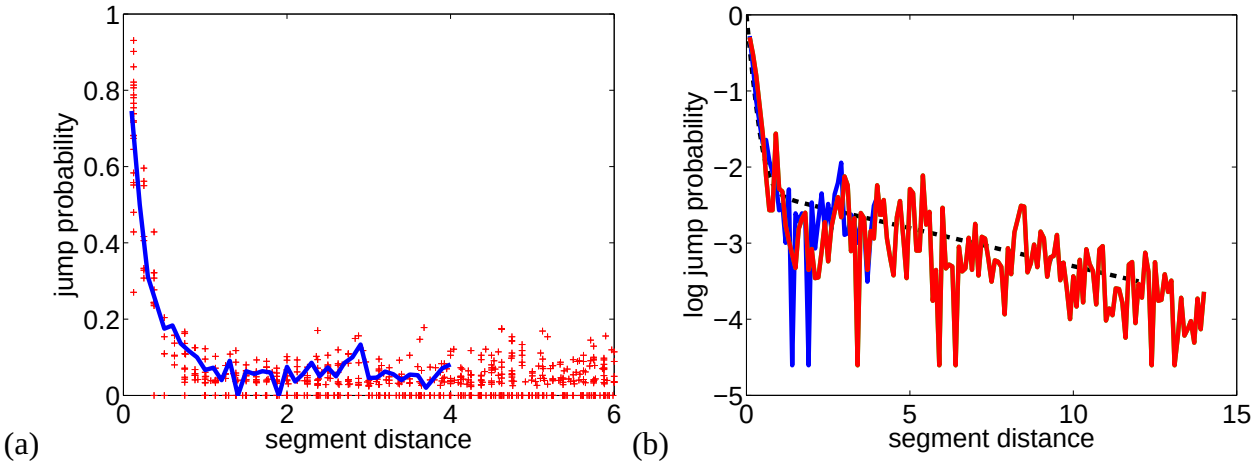

Figure 4: (a) Scatter plot of jump probabilities as a function of segment separation distance. Only segments with fault perpendicular separation distance at least as large as fault parallel separation distance are shown. Zero probability pairs are included as well, allowing for mean jump probability to be calculated, shown with solid line. (b) Functional form of mean jumping probability. Log jump probability versus linear distance. Straight line indicates exponential falloff. Functional form fit with two exponentials, one fast falloff at short distance, and one slower falloff at large distance. Dashed line shows exponential falloff Equation (1) fit with parameters $r_0 = .2$, $\epsilon = .08$, $r_1 = 10$. The two different color lines show two different domain sizes; they are hard to distinguish, and show the lack of dependence on domain size.